Internal Characterization of Magnetic Cores, Comparison to Finite Element Simulations: A Route for Dimensioning and Condition Monitoring

Sorelle Hilary Nguedjang Kouakeuo, Aurelie Solignac, Ruth Sabariego, Laurent Morel, Marie-Ange Raulet, Borel Toutsop, Pierre Tsafack, Benjamin Ducharne

Internal characterization of magnetic cores, comparison to finite element simulations: a route for dimensioning and condition monitoring

Sorelle Hilary Nguedjang Kouakeuo, Aurélie Solignac, Ruth Sabariego, Laurent Morel, Marie-Ange Raulet, Borel Toutop, Pierre Tsafack, Benjamin Ducharne

***Abstract*—Magnetic cores are typically used in every stage of an electrical energy production and distribution chain. Local defects, including edge burrs and interlaminar faults, are detrimental for system performance and should be detected swiftly to ensure high reliability and durability. Real-time magnetic core condition monitoring is a promising solution for rapid fault detection. However, similar to dimensioning or performance evaluation, this monitoring has always been performed through averaged magnetic properties, which limits efficiency. In this domain, significant progress is forecasted by achieving precise local measurements. In this study, an innovative solution is proposed to measure local magnetic properties, which is adapted to real-time monitoring and magnetic circuit evaluation. The proposed sensor is a one-piece device that is flat enough to be placed noninvasively between the laminations at distinct positions in the magnetic core. It measures the magnetic excitation and induction fields in two dimensions, which can be used as local inputs for real-time condition monitoring. In this manuscript, the proposed sensor was first detailed, experimental results were provided, and finite-element simulations were performed. The sensor capability was validated both experimentally and through simulation. The results of this study contribute to the development of an intelligent magnetic core that includes an effective real-time monitoring system. The study provides a local validation of the most advanced high-fidelity simulation method, which could be used to predict the responses of magnetic cores and electromagnetic converters to defects of various natures, as well as geometrical and property changes.**

***Index Terms*—Finite elements simulation, local defect, magnetic laminations stack, magnetic sensor, predictive maintenance.**

I. Introduction

Energy efficiency can play a crucial role in mitigating climate change. The rise in carbon dioxide emissions and the limited time available to achieve mitigation targets has aggravated the climate change problem. Improving the efficiency of electromagnetic devices can considerably contribute to achieving this target [1].

Numerous strategies, including novel geometrical designs, materials, technologies, have been proposed to improve electrical energy conversion rates. In this study, we focused on the magnetic conversion step, and particularly on the real-time control of the magnetic properties in the magnetic core at which energy transformation occurs [2], [3].

Most magnetic cores used to achieve energy conversions are composed of electrical steel sheet stacks. Electrical steel is an iron alloy designed for specific magnetic properties such as low power loss, high permeability. Even if some grades contain up to 6.5 wt% silicon, the content of most commercialized specimens remains close to 3 wt%. The silicon adjunction increases electrical resistivity, which reduces the induced eddy currents and magnetic losses (up to three times that of conventional steel) [4], [5].

Nonoriented electrical steel (NO FeSi) is produced without additional treatment to control crystal orientation. Close magnetic properties can be observed independently from the magnetization direction (quasi-isotropic behavior).

Electrical steel can be manufactured to develop optimal magnetic behavior in the rolling direction (RD). Anisotropy is generated through tight crystal orientation control (Goss texture [6]). After this treatment, iron silicon alloy becomes grain-oriented electrical steel (GO FeSi).

NO FeSi is cheaper than GO FeSi. NO FeSi is preferred when the cost is more critical than efficiency or for applications in which the magnetization direction is not set (such as electric

Sorelle Hilary Nguedjang Kouakeuo, Borel Toutsop and Pierre Tsafack are with the Faculty of Engineering and Technology, University of Buea, Buea, Cameroun.

Aurélie Solignac is with SPEC, CEA, CNRS, Université Paris-Saclay, CEA Saclay, 91191 Gif-sur-Yvette, France.

Ruth Sabariego is with KU Leuven, Dept. Electrical Engineering, Campus EnergyVille, 3600 Genk, Belgium.

Marie-Ange Raulet and Laurent Morel are with Laboratoire Ampère, Université de Lyon, 69621 Villeurbanne, France.

Benjamin Ducharne is with ELyTMaX IRL3757, CNRS, Univ Lyon, INSA Lyon, Centrale Lyon, Université Claude Bernard Lyon 1, Tohoku University, Sendai, Japan and with LGEF, Laboratoire de Génie Electrique et Ferroélectricité, INSA Lyon, France. e-mail: benjamin.ducharne@insa-lyon.fr.

motors and generators). GO FeSi is used in power and distribution transformers for maximum efficiency [7].

Electrical steel is produced in cold-rolled strips less than 2-mm thick. These strips are cut, coated, and stacked to form laminated magnetic cores. Various types of coating, including organic and inorganic, have been proposed. The coating layer maximizes the electrical resistance, limits the eddy current propagation, and provides corrosion resistance [8]. Stacking and coating electrical steel laminations have been used to considerably improve the efficiency of ferromagnetic cores.

However, the technique should be improved considerably; in 2014, the world databank estimated that 8% of the world's electrical energy production was lost between generation and consumption [9]. A considerable portion of this loss was attributed to magnetic conversion, hysteresis, and eddy current losses. Reducing losses from such conversions is critical for improving energy conversions.

During the machining processes, mechanical stresses can considerably affect magnetic properties. Furthermore, undesirable edge burrs around the cut edges and punched holes can be created, which results in interlaminar faults (ILFs) and negatively affects magnetic core efficiency [10]-[14]. ILFs can also occur during an operation because of multiple reasons, such as the vibration of loose windings, arcing from winding failure, transportation, and installation.

Magnetic core condition monitoring (MCCM) has been proposed to improve performance and durability [15], [16]. MCCM consists of a real-time inspection of the magnetic circuit performances to detect defects and predict a decrease in electromagnetic converter efficiency. MCCM has been performed by controlling the input and output electrical signals [15]. This simple approach limits the magnetic core diagnostic to average quantities and renders it impossible to geo-localize eventual defects. Considerable progress has been achieved in local magnetic measurements.

Numerous studies have focused on the conversion efficiency of magnetic cores (less than a year for [17]-[24]). However, most of these manuscripts are limited to simulation results. Some of the proposed techniques can be used to predict the local distribution of the magnetic fields, and like MCCM, these results were validated by comparing with averaged results. Furthermore, performance can be improved by locally measuring the magnetic behavior in the magnetic core.

For geometrical problems, current laminated magnetic core characterizations are limited to either global information (averaged through the cross-section) or surface observations [2], [14], [25]. Embedding any instrumentation system inside a laminated magnetic core was difficult. In [26] and [27], printed electronics have been used to perform such measurements.

In [27], we specifically focused on embedding a $\overrightarrow{B_a}$ sensor (where $\overrightarrow{B_a}$ is the magnetic flux density (induction field) averaged through the tested specimen cross-section). We used the printed magnetic needle probes method (PMNPM) (also described in [28]), in which the conventional needle probe [29], [30] is replaced with a printed probe. The resulting sensor exhibits a thickness of a conductive ink layer (≈30 µm). In [27], a 270-µm thick chip composed by a giant magneto resistance (GMR) sensor [31], [32] was positioned next to the PMNPM sensor to measure the surface tangent magnetic excitation field $\overrightarrow{H_{surf}}$ locally. Local hysteresis cycles $B_{a_i}(H_{surf_i})$ were plotted for each lamination (all sensors were placed in positions where $\overrightarrow{B_a}$ and $\overrightarrow{H_{surf}}$ are presented collinearly). Experimental characterizations were validated by summing all local measurements and comparing them to averaged values obtained with wound coils. Although excellent results were obtained, some concerns, including the thickness of the GMR sensor (it was still too high compared to the thickness of the coating and of the electrical steel sheets), remained. Furthermore, electrical contacts between the printed part and the acquisition device were ensured using a 100-µm thick bondable terminals, which created a small bump on the lamination edge.

In this study, we performed magnetic core local characterization using a novel method. A novel sensing solution was proposed to address the problems of the previous methods. This solution was described and validated in the second section of this manuscript. In the third section, the measurements were validated using local simulation results obtained using the open-source Onelab® software suite [33] (finite-element software and mesh generator).

In Onelab®, finite elements are combined with vector hysteresis material laws to realize the most advanced high-fidelity simulation method.

An experimental validation of the simulation method was performed [34] to confirm the predictive capability of the proposed method. Discussions and conclusions are provided in the last section of the manuscript.

II. $B_A(H_{SURF})$ Local Characterization of an Electric Steel Magnetic Core Using Embedded Sensors.

A. Magnetic Induction Measurement

The magnetic needle probe method (MNPM) is used to record magnetic flux variations in a ferromagnetic laminated core by surface measurement. MNPM is based on the potential difference measured by two conductive needles in contact with the surface of a ferromagnetic laminated core (Fig. 1). The potential difference can be attributed to eddy currents circulating in the lamination cross-section during the magnetization process [35].

From its first description by Werner in 1949 [36] and up to its most recent published version (2020-21 [22]-[24]), numerous studies have focused on an accurate description of the ideal experimental conditions to ensure accuracy and MNPM reproducibility:

_ As described in [35], the voltage drop between positions 1 and 2 in Fig. 1 below can be approximated by using the following expression:

$$V_{12} \approx \frac{1}{2}\int_{S_{1234}} \frac{\partial B_{1234}}{\partial t} \cdot dS_{1234}, \quad (1)$$

where B_{1234} and S_{1234} are the induction magnetic field and the cross-section through positions 1, 2, 3, and 4 (blue mesh in Fig. 1), respectively.

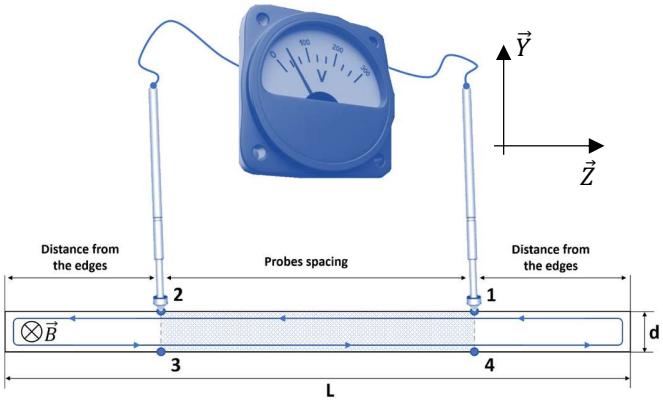

Fig. 1 Schematic of the magnetic needle probe method (MNPM).

In order to correctly use the needle probe sensor, the following specifications must be met:
1) For accurate measurements, the distance **1**-**2** should be higher than 10 mm [29].
2) The distance from the edges should be higher than half of the specimen thickness (d/2) [29].
3) The leakage flux in the enclosed near-surface magnetized air should be negligible [37], [38].
4) The probe's distance to the specimen ratio (**1**-**2**/d) should be significant [39].

The application of MNPM is limited because of weak electromotive forces, especially in the low-frequency range. However, considerable advances have been achieved in analog and digital electronics. Improvements in the MNPM have resulted in numerous applications, such as local nonuniform electromagnetic field investigations [40], [41], cutting-edge stress [42], [43], stress-induced peening processes [44], and homogenization analysis in lamination stacks [45]. PMNPM, as described in [26], satisfies all the aforementioned conditions. The test probe can be replaced with a printed conductive layer, which results in a leakage flux that is negligible. The thickness of the whole sensor (a conductive ink layer, ≈30 µm) also becomes irrelevant.

B. Magnetic Excitation Measurement

The PMNPM is a nonintrusive method for measuring a local directional flux variation through the cross-section of a laminated core. Here, B_a is obtained from time-based integration. For a complete hysteresis cycle plot, H_{surf} should be recorded using small dimensions GMR sensors. GMRs can be used to detect up to less than a few nanoteslas beyond substantial frequency and temperature ranges [31]. GMRs consist of multiple thin layers, including two ferromagnetic deposited thin films isolated by a metallic nonmagnetic spacer. The total active part thickness is typically smaller than 100 nm.

The first ferromagnetic layer, which is the reference layer (or fixed layer), functions as a permanent magnet. The second ferromagnetic deposit (the free or nonfixed layer) is magnetically soft. The magnetic state of the layer fluctuates under the influence of external magnetic excitations. These variations induce overall resistance fluctuations because of the spin-dependent charge transport phenomena [46]-[48]. The linearity of the GMR is set by the shape anisotropy in the free layer. This anisotropy induces an easy magnetization direction at 90° of the fixed layer magnetization [31]. The GMR sensor is sensitive to the in-plane field and along the magnetization of the fixed layer.

For additional information on the GMR working principles, please refer to [48].

C. Complete Low-Thickness Sensing Solution

For GMR deposition, the roughness of the substrate should be less than 1 nm rms. Under such a condition, a direct implementation is not possible on a ferromagnetic electrical steel lamination whose roughness is approximately tens of nanometers in the best cases. In [27], a 270-µm thick silicon substrate was used to develop a noninvasive solution. Such a high thickness is not feasible. However, polishing treatments or fabrications process can be performed [46]. Although these methods were not tested in [27], the resulting substrate thickness can decrease to a few tens of micrometers.

As mentioned in the Introduction, PMNPM deposition is associated with thickness concerns on the edges of the lamination stack because of electrical contacts. In this study, we solved this problem and improved the overall electrical connections by depositing the GMR and printing the needles probe on the same patch. Fig. 2 (right) displays the layout of the resulting sensor, including both the magnetic induction and excitation measurement in RD and transverse direction (TD). Fig. 3 displays a photograph of the resulting measuring sensor proposal.

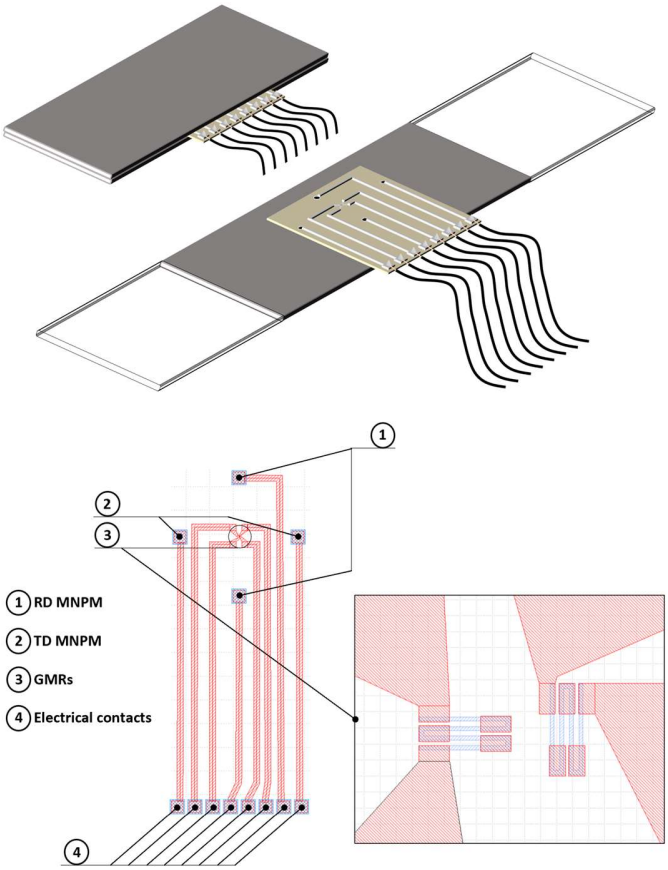

Fig. 2 MNPM/GMR sensor; left: illustration of the electrical contacts, right: whole sensor layout.

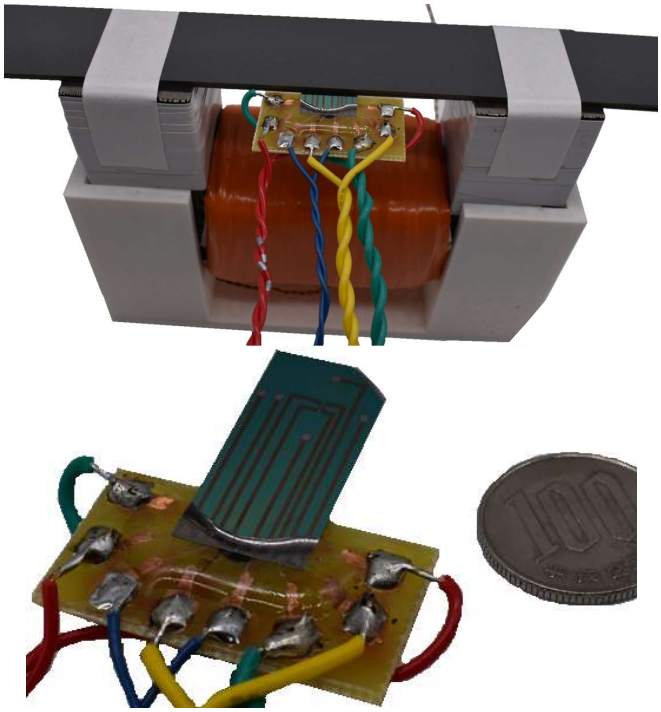

Fig. 3 Photograph of the MNPM/GMR sensors and resulting single patch.

As displayed in the three-dimensional (3D) illustrations in Fig. 2 (left) and confirmed in the photographs in Fig. 3, all the electrical contacts (large pads) were placed on the bottom part of the sensor patch located outside the lamination stack. An additional local layer of conductive ink deposed in a final fabrication step ensured needle probe electrical contacts. The coating was removed locally on the bottom face of the tested lamination. Contact resistances were characterized from 20 Hz to 1 kHz and for temperatures varying from 20 to 200 °C. However, these results were inferior to 0.5 Ω for all the tests and minimal compared with the 10^6 Ω acquisition device input impedance, which render their influence negligible. The Si/SiO_2 (500)//Ta (3)/$Ni_{80}Fe_{20}$ (6.3)/$Co_{90}Fe_{10}$ (2.1)/Cu (2.9)/$Co_{90}Fe_{10}$ (2)/Ru (0.85)/$Co_{90}Fe_{10}$ (2)/$Ir_{22}Mn_{78}$ (7.5)/Ru (0.4)/Ta (5) (thicknesses in nanometers) GMRs were deposited through sputtering (Rotaris–Singulus) on 270-µm thick oxidized silicon wafers. Standard UV lithography techniques were used to fabricate meander-shaped GMR structures with metallic contacts (100 nm of Ta/cu/Ta), as displayed in the enlarged image of Fig. 2. The probe contains two magnetic tips and two GMR sensors for vector field measurements. The axis of sensitivity of the GMR could be changed by varying local courant pulse heating under a field [46].

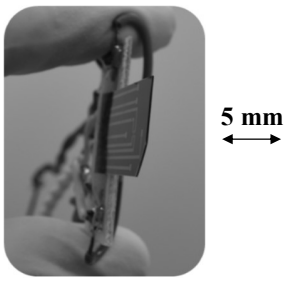

Fig. 4 Sensor patch resulting thickness.

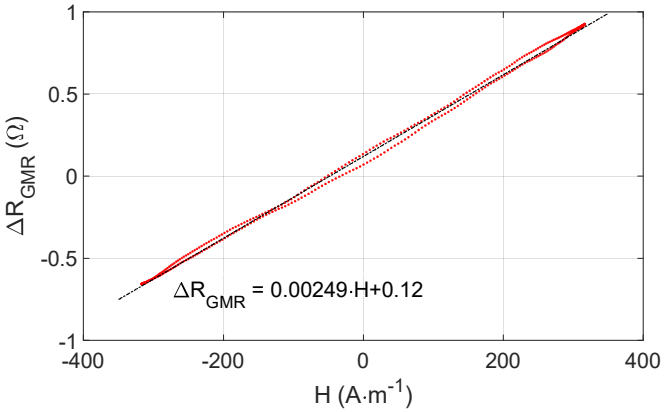

Fig. 5 Precharacterization of GMR sensors (R_0 = 630 Ω), linearity, and sensitivity estimation.

The thickness of the patch was 270 µm (Fig. 4), but it could be easily reduced through CMP polishing or silicon on insulator process [46] to less than 30 µm. However, because of the extreme fragility of the resulting sensor, processing must be performed meticulously.

The sensitivity and linearity of the GMRs have been evaluated in an initialization stage using Helmholtz coils. The results of this precharacterization are displayed in Fig. 5.

The proximity of the GMR to the tested ferromagnetic sheet in the final configuration is also crucial. Commercially available hall effect sensors are used for performing tangent surface excitation field measurements in classical approaches. However, the field gradients above the specimen surfaces are critical, and the hall sensors used are too bulky to provide reliable information. This concern has been discussed in many publications, including [49], [50], and complex alternative solutions have been proposed [51]. The GMR sensors described in this study provide close measurements and ensure excellent H_{surf} observation.

D. Experimental Validation

The experimental setup used to validate the new sensing solution has been comprehensively described in [26] and [27]. The IEC 60404-3 standard defines the use of a single-sheet tester to characterize electrical steel lamination [52], even if differences exist, such as in the use of a single yoke, the yoke dimensions, the primary winding being wound around the yoke instead of the tested specimens, and a stack of 10 laminations replacing the single sheet of electrical steel for stack tests. The experimental setup of this study was established using this standard.

All the GO FeSi specimens tested were picked up from the same batch. As provided by the manufacturer and previously characterized by the team [26], [27], their physical properties at room temperature are displayed in Table 1.

Table I Typical FeSi GO magnetic Properties

	Comp.	μr_{max}	Hc (A·m^{-1})	Js (T)	Tc (°C)	$\lambda_s = (\Delta l/l)_{Js}$
GO FeSi	Fe_{97}–Si_3	15–80 x 10^3	4–15	2.02	750	1–3 x 10^{-6}

Here μr_{max}, Hc, Js, Tc, and λ_s are the relative permeability, coercivity, saturation polarization, the Curie temperature, and the magnetostriction coefficient, respectively. Here, l is the initial length and Δl is the length variation at saturation.

	Core loss (W/kg)					
	W10/50	W10/400	W10/1k	W5/2k	W1/10k	W0.5/20k
GO FeSi	0.7	14.4	62.0	50.2	38.0	33.0

W10/50 is the core loss at 50 Hz, 1 T (10 kGauss)

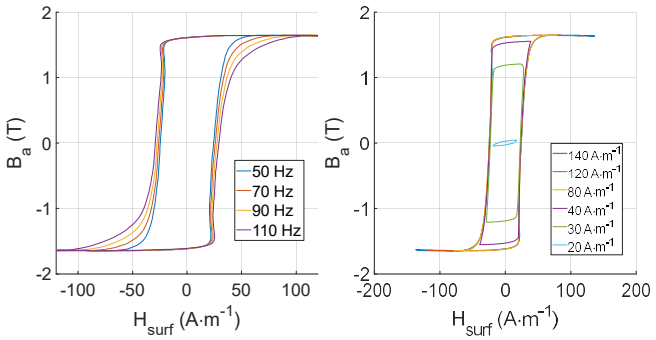

Fig. 6 Single lamination tests (left: vs. frequency, max (H_{surf}) = 120 A·m^{-1}, right: vs. H_{surf} amplitude, f = 50 Hz).

In the first experimental tests, a single instrumented ferromagnetic sheet was laid on the yoke. Measurements with the sensor patch were monitored at various frequencies and amplitudes. The experimental results are displayed in Fig. 6. The sensor size allows measurement in the middle of the lamination far from the edges at which inconsistency in the MNPM could affect measurements [29]. Thus, all measurements were performed in the central zone of the laminated sheet. The 2D capability of the sensing solution was tested subsequently by positioning the sensor patch at 45° (Fig. 7). As displayed in Fig. 8, when the angle corrections were processed (projections), similar results were obtained in the x- and y-direction, which confirmed the 2D performance of the sensor patch. This first series of tests were completed to verify the cohesion between the experimental results and the manufacturer information. Next, a pile of 10 electrical steel laminations, including the instrumented laminations, was used to validate the sensor in a stack configuration. The instrumented sheet was moved in every stack position, and various excitation levels and frequencies were tested. Some of these results are included in the next section. All tests were performed at room temperature.

III. Internal Magnetic Behavior of a Laminated Core: Comparison to Finite Elements Simulation Results

Numerous simulation methods have been developed to predict the magnetic behavior and electric characteristics of electromagnetic devices. Simulations can be used in a phenomenological manner to improve the knowledge and interpretation based on experimental results [53]. Simulations can also be used to predict quantities and information beyond reach, including the effect of potential defects on the overall electromagnetic converter behavior [54]. Numerical computations can avoid fastidious (and often expensive) experimental campaigns during the dimensioning phase.

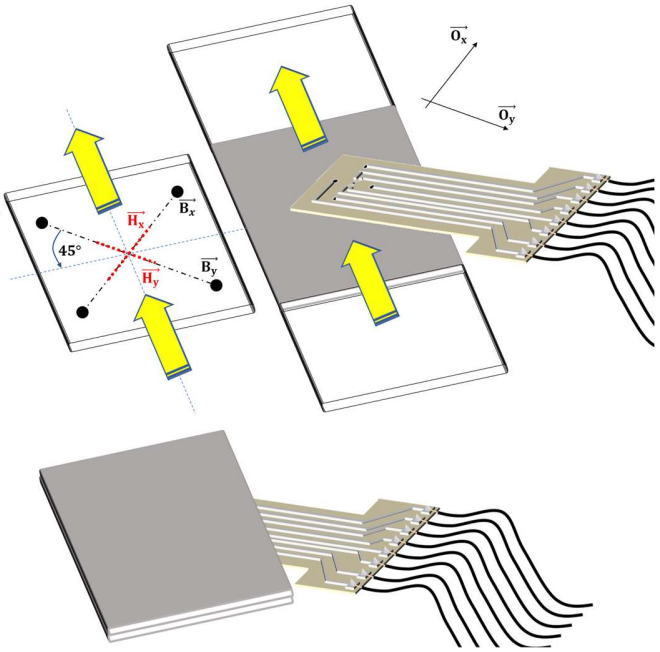

Fig. 7 Two-dimensional measurement verification and illustration of the sensor positioning.

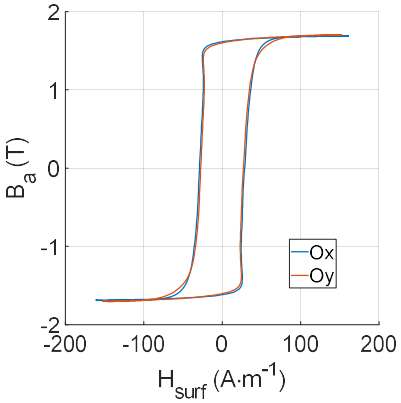

Fig. 8 Superimposition of the hysteresis cycles measured on both axis $\overrightarrow{O_x}$, $\overrightarrow{O_y}$ (see Fig. 7 for experimental conditions illustration).

In electromagnetic devices design, simulation methods based on the space discretization to solve partial differential equations, such as the finite elements method (FEM), are highly promoted because of features such as their versatility, complex geometries, local material characteristics, and nonlinearities. In the specific case of electrical steel lamination stacks, FEM has typically been used to predict the local distribution of the magnetic fields [55]-[60], including the magnetic core where previous instrumentation could not reach. In these studies, the experimental validation was not systematic and averaged results at the core level (usually, the magnetic losses) are always used, as displayed in Fig. 26 of [60] or Fig. 5 of [57].

In the previous section, a sensing solution sufficiently thin to be embedded between the laminations of a magnetic core and return local information has been described. In this section, FEM simulation results are analyzed. By comparing the experimental and numerical results, we validated both the practical and numerical methods.

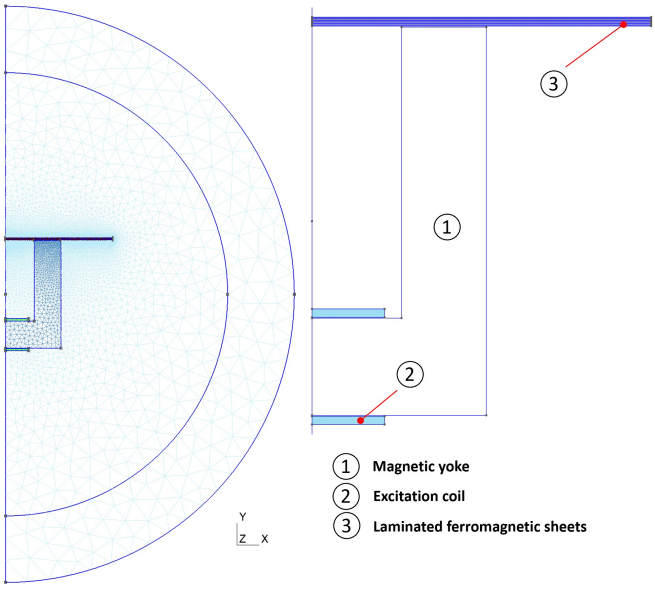

Fig. 9 Two-dimensional planar, symmetric simulation domain, and its mesh (left) with spherical shell (outer ring) to account for infinity; detail of the electromagnet circuit (right).

A. Description of the Simulation Method

The magnetic yoke, lamination stack, and excitation coil were investigated. We developed a 2D planar FEM magneto dynamic model (Fig. 9) based on the classical magnetic vector potential formulation within the open-source Onelab® software suite [33]. We used the symmetry (half electromagnet circuit) and a shell transformation (no truncation) to detail their infinity. A homogeneous current density crossed the excitation coil $j_s(x,y,t)$. A set of 10 laminations was considered. The vectorial Jiles–Atherton model described in [61], a variant of the model first proposed by Bergqvist [62], was applied as the material law in the ferromagnetic parts. This extension was not feasible for anisotropic materials such as FeSi GO tested in the study.

However, the comparisons with the experimental observations were limited to the X-axis direction and far from the yoke legs, where B_a and H_{surf} are assumed in RD and colinear. The hysteresis simulation parameters are presented in Table 2. These parameters were set according to the RD behavior in pre-processing through optimization and comparisons with quasi-static experimental results. According to the Jiles–Atherton theory of ferromagnetism, α quantifies the interdomain coupling, a is the domain walls density, k is the average energy to break the pinning sites, and c is magnetization reversibility [63].

Table 2 Jiles–Atherton (J–A) simulation parameters for FeSi GO (RD).

J-A parameters	Typical value
a (A.m^{-1})	4
Ms (A.m^{-1})	1312000
k (A.m^{-1})	40
c	0.01
α	7.4 10^{-6}

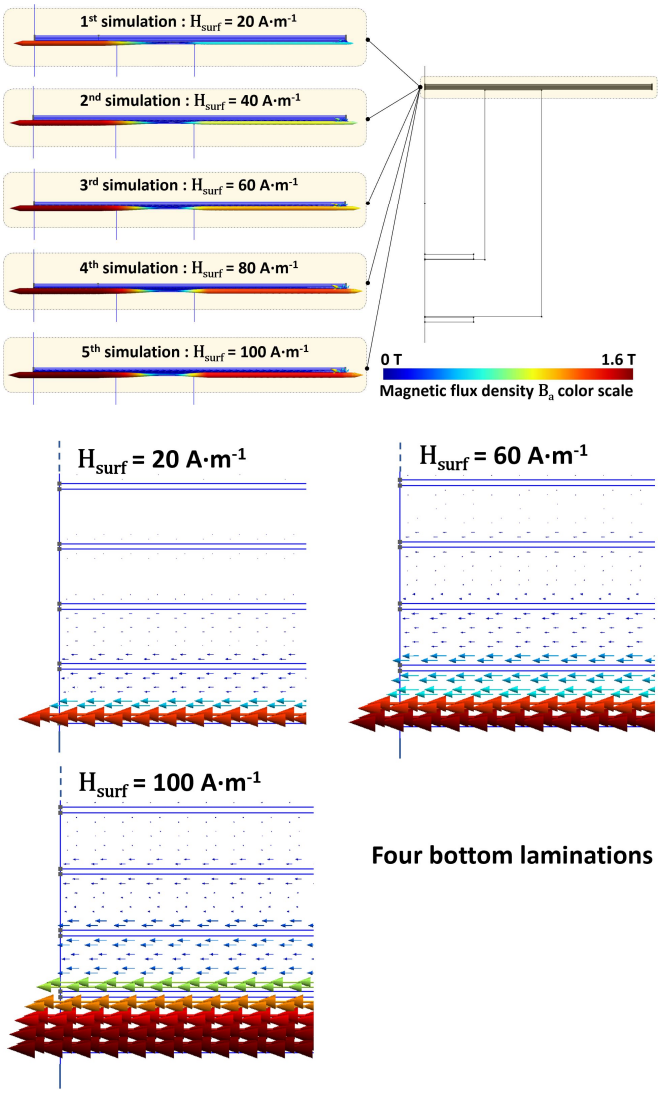

Fig. 10 Simulation of the magnetic induction (B) in the stack of laminated sheets, H_{surf} varying from 0 to 100 A·m^{-1}.

B. Simulation Results and Comparisons With Experimental Results

To test the simulation and the measurement methods in the worst-case scenario, we intentionally set the electrical current in the excitation coil to produce a significant gradient of magnetic induction between the first and the last laminated sheet of the stack. The simulated evolution of the magnetic induction in the magnetic stack when H_{surf} varies from 0 to 100 A·m^{-1} is given in Fig. 10.

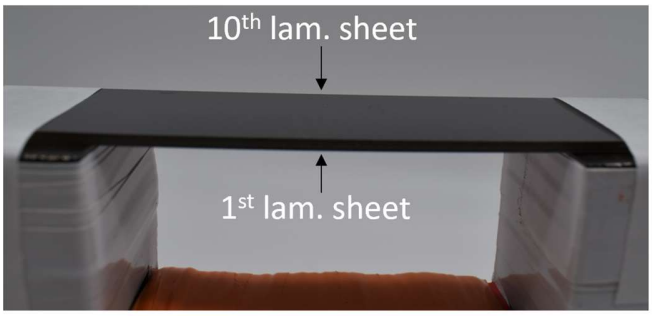

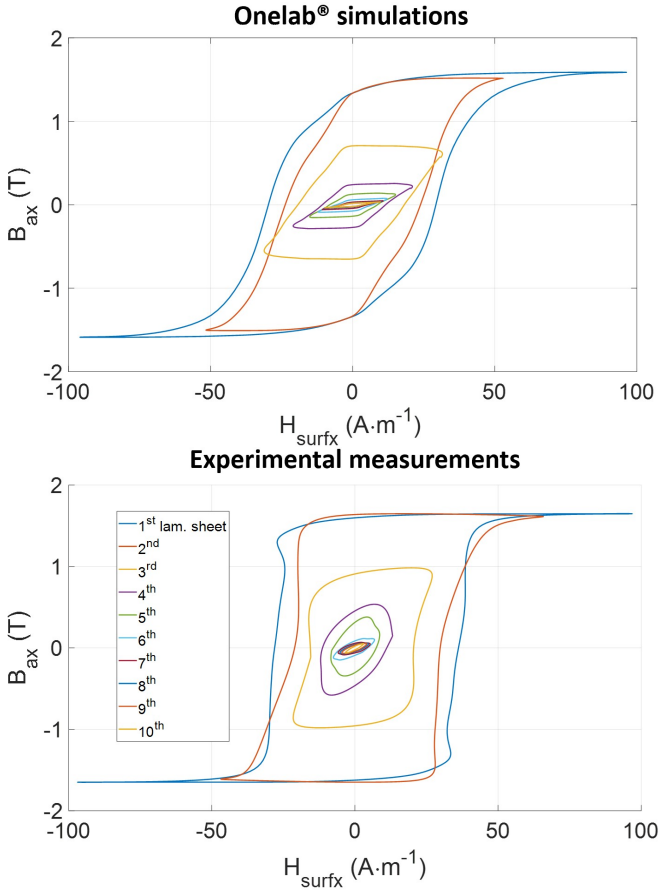

Fig. 11 Comparisons of the Onelab® simulations and experimental results in local tests.

Fig. 11 presents a comparison of the magnetic hysteresis cycles simulated and measured for every ferromagnetic lamination during a full magnetization cycle.

Even if the resulting hysteresis cycles are not identical (probably because of an imperfect estimation of the J-A model parameters or to the simulation hypothesis), the close evolution of the magnetic gradient is notable. The predictive capability of the simulation method is evident in Fig. 13, in which comparisons were proposed for the variation of a series of hysteresis cycle indicators (Fig. 12) as a function of the magnetic sheet position.

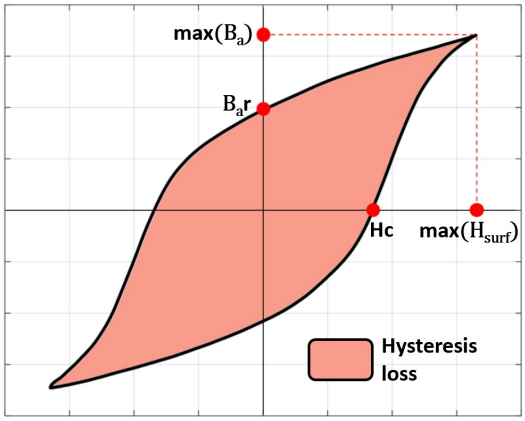

Fig. 12 Series of hysteresis cycle indicators tested.

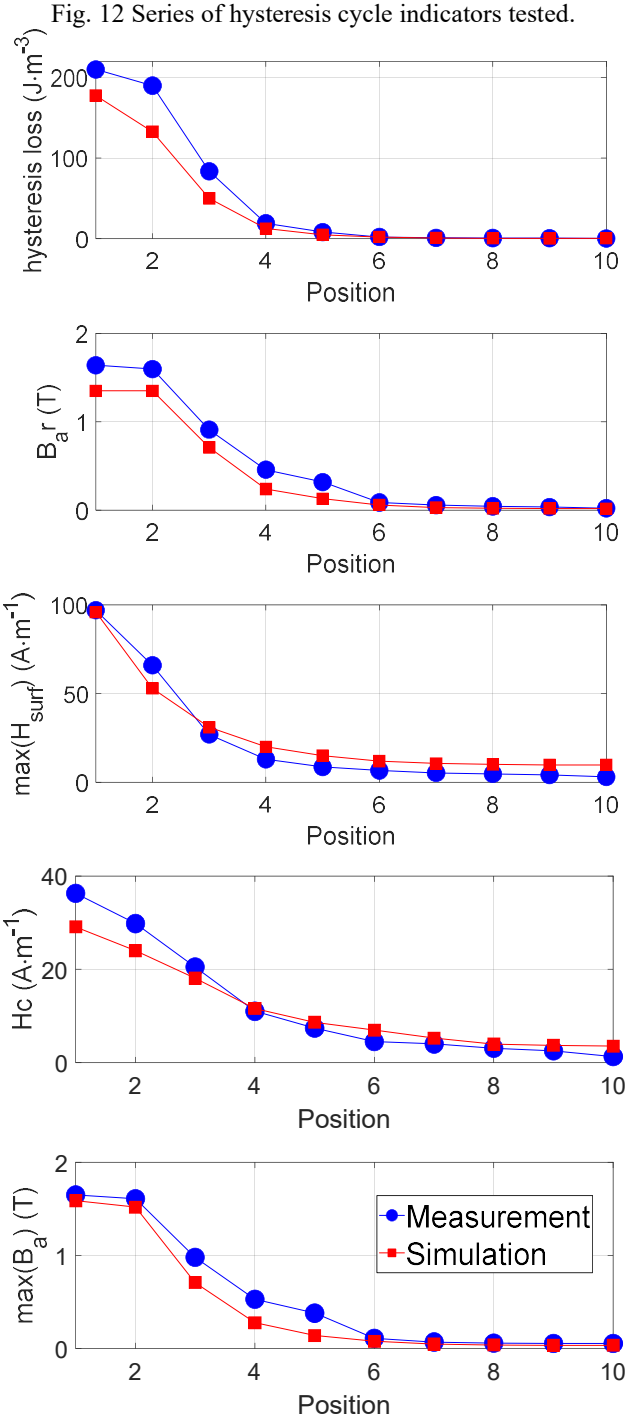

Fig. 13 Comparison measurements/simulations for the main hysteresis cycle indicators versus the magnetic sheet position.

A depression was observed in the hysteresis cycles of the first, second, and third positions. Such behavior has already been noted in literature and associated with the dynamic losses during the magnetization process [64], [65].

Finally, the uncertainty marker defined in Eq. 2 was applied to the five tested indicators to verify the global performance of the proposed simulation method. The results are presented in Table 3.

$$\text{Error (\%)} = \frac{1}{m} \cdot \sum_{i=1}^{m} \frac{\left|x_i^{sim} - x_i^{meas}\right|}{x_i^{meas}} \cdot 100\% \qquad (2)$$

Table 3 Quantitative evaluation of the simulation method (m = 10 is the laminations number).

	Error (%)
Hysteresis loss	22
Hc	14.5
B_{ar}	32
max(B_a)	29.6
max(H_{surf})	32.7

Table 3 details the large errors between the simulation predictions and the experimental results. However, the Eq. 2 error definition is the average value of the relative error calculated on the ten sheet positions. Considerably lower error percentages could have been obtained by limiting those calculations to the bottom laminations at which the magnetic flux density is concentrated. The error is small for the first sheets (positions 1, 2, and 3). The measured magnetic quantities exhibit significant values for these positions and lead to a consequent ratio between the valuable signal and ambient noise. From laminations 4 to upwards, the induction levels are in the same range as PMNP uncertainty. For these positions, the comparisons are inaccurate and considerably alter quantitative evaluation. Different paths can be followed to improve these results: from the simulation perspective, alternative vectorial hysteresis models have been described in scientific literature [24], [66]-[67]. Accuracy was claimed to be improved and will be evaluated in the future. Furthermore, the evaluation of the simulation parameters can be improved. Eventually, from the practicality perspective, the calibration of the GMR sensors and the signal treatment of PMNP can be improved.

IV. Conclusion

Energy efficiency and reliability have attracted considerable research attention. Magnetic cores are essential elements of electrical energy production and distribution. Even if these methods have been thoroughly studied, further improvements is necessary.

Local characterizations of the magnetic behavior in the magnetic core should be investigated. Technical limitations have constrained such measurement. However, simulation tools have been proposed for prediction. Moreover, validation have been compared with average or surface observations, and local verifications were expected.

A 100-µm thick patch sensor (whose thickness can be reduced) combining MNPM and GMR sensors was proposed to provide in-plan magnetic characterization inside a ferromagnetic laminated sheet stack. The patch was tested first on a single ferromagnetic laminated sheet. A 2D measurement was proposed by comparing the two pairs of sensors in an experimental condition that required the sensor to provide the same information. Next, stack tests were performed by positioning the sensor patch between every laminated sheet. Subsequently, comparisons with time-domain FEM simulations were proposed and used as validation for both the experimental and the simulation tools.

Even if the proposed patch sensor provided accurate local measurements in all the performed tests, the authors have noted the following limitations:

1) The PMNP electrical contacts were ensured from an additional layer of conductive ink processed in a further fabrication step. However, this solution is not optimal, and alternatives should be determined.

2) The fragility of the sensor patch was the most critical concern for high technology readiness level (TRL) developments. The thinned patch should be handled meticulously, especially during polish treatments. The use of flexible substrates is plausible but constitutes time-consuming developments beyond the scope of this project.

A flexible substrate is the long-term objective of this study. The following short-term prospects exist:

1) To test the sensor patch in a real-life situation. An instrumented power transformer was designed, including multiple sensor patches dispatched all over the transformer laminated magnetic core.

2) To evaluate the detection of ILFs or edge burrs with the sensor patch. A specific experimental setup including well-known defects should be designed for this purpose.

References

[1] J.M. Silveyra, E. Ferrara, D.L. Huber, T.C. Monson, "Soft magnetic materials for a sustainable and electrified word," *Science,* vol. 362, eaao0195, 2018.

[2] F. Fiorillo, "Measurements of magnetic materials," *Metrologia,* vol. 47, n° 2, 2010.

[3] A.J. Batista, J.C.S. Fagundes, P. Viarouge, "An automated measurement system for core loss characterization," *IEEE Trans. Inst. Meas.,* vol. 48, n° 2, pp. 663 – 667, 1999, Art no. 6281257.

[4] J. Gyselinck, L. Vandevelde, J. Melkebeek, P. Dular, F. Henrotte, W. Legros, "Calculation of eddy currents and associated losses in electrical steel laminations," *IEEE Trans. Magn.,* vol. 35, n° 3, pp. 1191 – 1194, 1999.

[5] G. Bertotti, "Hysteresis in magnetism," Academic Press, Boston, 1998.

[6] N.P. Goss, US Patent, N° 1,965,559, 1934.

[7] R.M. Bozorth, "Magnetism," Enc. Brit., vol. 14, pp. 636 – 667, 1957.

[8] Beatty, Standard Handbook for Electrical Engineers 11th ed., pg. 4-111.

[9] The world databank.

[10] C. A. Schulz, S. Duchesne, D. Roger, J. Vincent, "Short Circuit Current Measurements Between Transformer Sheets," *IEEE Trans. Magn.,* vol. 46, no. 2, pp. 536 – 539, 2010.

[11] R. Mazurek, H. Hamzehbahmani, A. J. Moses, P. I. Anderson, F. J. Anayi and T. Belgrand, "Effect of Artificial Burrs on Local Power Loss in a Three-Phase Transformer Core," *IEEE Trans. Magn.,* vol. 48, no. 4, pp. 1653 – 1656, 2012.

[12] H. Hamzehbahmani, P. Anderson, J. Hall and D. Fox, "Eddy Current Loss Estimation of Edge Burr-Affected Magnetic Laminations Based on Equivalent Electrical Network—Part I: Fundamental Concepts and FEM Modeling," *IEEE Trans. on Pow. Deliv.*, vol. 29, no. 2, pp. 642 – 650, 2014.

[13] H. Hamzehbahmani, P. Anderson, J. Hall and D. Fox, "Eddy Current Loss Estimation of Edge Burr-Affected Magnetic Laminations Based on Equivalent Electrical Network—Part II: Analytical Modeling and Experimental Results," *IEEE Trans. on Pow. Deliv.*, vol. 29, no. 2, pp. 651 – 659, 2014.

[14] S. B. Shah, O. Osemwinyen, P. Rasilo, A. Belahcen, and A. Arkkio, "Thermographic measurement and simulation of power losses due to interlaminar contacts in electrical sheets," *IEEE Trans. Inst. and Meas.*, vol. 67, no. 11, pp. 2628–2634, 2018, Art no. 6003409.

[15] H. Hamzehbahmani, "A Phenomenological Approach for Condition Monitoring of Magnetic Cores Based on the Hysteresis Phenomenon," *IEEE Trans. Inst. and Meas.*, vol. 70, pp. 1 – 9, 2021, Art no. 6003409.

[16] H. Hamzehbahmani, "An experimental approach for condition monitoring of magnetic cores with grain-oriented electrical steels," *IEEE Trans. Inst. and Meas.*, vol. 69, no. 6, pp. 3395–3402, 2020, Art no. 19610784.

[17] S.M. Plotnikov, "Determination of eddy-current and hysteresis losses in the magnetic circuits of electrical machines," Meas. Tech., vol. 63, pp. 904 – 909, 2021.
[18] S.Q. Antonio, F. R. Fulginei, A. Laudani, A. Faba, E. Cardelli, "An effective neural network approach to reproduce magnetic hysteresis in electrical steel under arbitrary excitation waveforms," *J. Magn. Magn. Mater.,* vol. 528, 167735, 2021.
[19] M. Shi, A. Qiu, J. Li, "Vector magnetic properties of electrical steel sheet under DC-biased flux and rotating magnetic fields of varying frequencies," *IEEE Trans. Magn.,* 2021.
[20] L.M. Duarte, J.D. de Alencar Santos, F. Nélio Costa Freitas, P. Pedrosa Rebouças Filho, H. Ferreira Gomes de Abreu, "A novel approach based on pattern recognition techniques to evaluate magnetic properties of a non-grain oriented electrical steel in the secondary recrystallization process," *Measurement,* vol. 167, 108135, 2021.
[21] Z. He, L. Zhu, Z. Wang, C-S. Koh, "Anomalous loss and hysteresis loop in electrical steel sheet," *IEEE Trans. Magn.,* vol. 57, n° 6, pp. 1 – 4, 2021.
[22] W. Mazgaj, M. Sierzega, Z. Szular, "Approximation of hysteresis changes in electrical steel sheets," *Energies,* 14(14), 4110, 2021.
[23] S. Zhang, B. Ducharne, S. Takeda, G. Sebald, T. Uchimoto, "Low-frequency behavior of laminated electric steel sheet: investigation of ferromagnetic hysteresis loops and incremental permeability," *J. Magn. Magn. Mater.,* vol. 538, 168278, 2021.
[24] B. Ducharne, S. Zurek, G. Sebald, "A universal method based on fractional derivatives for modeling magnetic losses under alternating and rotational magnetization conditions," *J. Magn. Magn. Mater.,* Vol. 550, 169071, 2022.
[25] S. Imamori, S. Steentjes, K. Hameyer, "Influence of interlocking on magnetic properties of electrical steel laminations," *IEEE Trans. Magn.,* vol. 53, n° 11, pp. 1 – 4, 2017.
[26] S.H. Nguedjang Kouakeuo, Y.A. Tene Deffo, B. Ducharne, L. Morel, M.A. Raulet, P. Tsafack, J.M. Garcia-Bravo, B. Newell, "Embedded printed magnetic needle probes sensor for the real-time control of the local induction state through a laminated magnetic core," *J. Magn. Magn. Mater.,* Vol. 505, 166767, 2020.
[27] S.H. Nguedjang Kouakeuo, B. Ducharne, A. Solignac, L. Morel, M.A. Raulet, B. Toutsop, Y.A. Tene Deffo, P. Tsafack, "Non-invasive local magnetic hysteresis characterization of a ferromagnetic laminated core," *J. Magn. Magn. Mater.,* vol. 527, 167783, 2021.
[28] B. Ducharne, Y.A Tene Deffo, P. Tsafack, S.H. Nguedjang Kouakeuo, "Directional Barkhausen noise magnetic measurement using the magnetic needle probe method," *J. Magn. Magn. Mater.,* vol. 519, 167453, 2021.
[29] T. Yamaguchi, K. Senda, M. Ishida, K. Sato, A. Honda and T. Yamamoto, "Theoretical analysis of localized magnetic flux measurement by needle probe," *J. Physique IV,* 8 717–20 Pr2, 1998.
[30] G. Loisos, A. J. Moses, "Demonstration of a new method for magnetic flux measurement in the interior of a magnetic material," *Sens. and Act. A: Phys.,* vol. 106, iss. 1 – 3, pp. 104 – 107, 2003.
[31] J. Moulin, A. Doll, E. Paul, M. Pannetier-Lecoeur, C. Fermon, N. Sergeeva-Chollet, A. Solignac, "Optimizing magnetoresistive sensor signal-to-noise via pinning field tuning," Appl. Phys. Lett., vol. 115, 122406, 2019.
[32] M. Hauser, L. Kraus, P. Ripka, "Giant magnetoimpedance sensors," *IEEE Trans. Inst. and Meas.*, vol. 4, pp. 28 – 32, 2001, Art no. 6973177.
[33] C. Geuzaine, F. Henrotte, J.-F. Remacle, E. Marchandise, R. Sabariego, "ONELAB Open numerical engineering laboratory," in 11e Colloque National en Calcul des Structures, Giens, France: CSMA, 2013.
[34] D.M. Sullivan, "Electromagnetic simulation using FDTD method," NJ, Piscataway: Wiley-IEEE Press, 2000.
[35] G. Loisos, A.J. Moses, "Critical evaluation and limitations of localized flux density measurements in electrical steels," *IEEE Trans. Magn.,* vol. 37, n° 4, pp. 2755 – 2757, 2001.
[36] E. Werner, Austrian Patent n° 191015, 1949.
[37] K. Senda, M. Ishida, K. Sato, M. Komatsubara, T. Yamaguchi, "Localized magnetic properties in grain-oriented silicon steel measured by stylus probe method," *Trans. IEE Japan,* pp. 941 – 950, 1997.
[38] K. Senda, M. Ishida, K. Sato, M. Komatsubara, T. Yamaguchi, "Localized magnetic properties in grain-oriented electrical steel measured by needle probe method," *Electr. Eng. Japan,* vol. 126, pp. 942 – 949, 1999.
[39] K. Matsubara, T. Nakata, Y. Kadota, "A novel method of measurements of magnetic flux in silicon steel sheet with magnetic flux leakage," Nat. Conf. IEEE Japan, 1988.
[40] M. Enokizono and I. Tanabe, "The problem of simplified two-dimensional magnetic measurement apparatus," in 5th International Workshop on 1 and 2-Dimensional Magnetic Measurement and Testing, 1999.
[41] A. A. Abdallh, P. Sergeant, G. Crevecoeur, L. Vandenbossche, L. Dupre, M. Sablik, "Magnetic Material Identification in Geometries With Non-Uniform Electromagnetic Fields Using Global and Local Magnetic Measurements," *IEEE Trans. on Mag.,* vol. 45, n° 10, pp. 4157 – 4160, 2009.
[42] A. A. Abdalh, L. Dupré, "Local magnetic measurements in magnetic circuits with highly non-uniform electromagnetic fields," *Meas. Sci. Tech.,* vol. 21, n°4, 2010.
[43] G. Loisos, "Novel flux density measurement methods of examining the influence of cutting on magnetic properties of electrical steels," Ph.D. thesis, Cardiff University, UK, 2002.
[44] G. Crevecoeur, L. Dupre, L. Vandenbossche, R. Van de Walle, "Local identification of magnetic hysteresis properties near cutting edges of electrical steel sheets," *IEEE Trans. on Mag.,* vol. 44, n°6, pp. 1010 – 1013, 2008.
[45] Y.A. Tene Deffo, P. Tsafack, B. Ducharne, B. Gupta, A. Chazotte-Leconte, L. Morel, "Local measurement of peening-induced residual stresses on Iron Nickel material using needle probes technique," *IEEE Trans on Mag.,* vol. 55, iss. 7, 7100208, 2019.
[46] C. Chopin, J. Torrejon, A. Solignac, C. Fermon, P. Jendritza, P. Fries, M.Pannetier-Lecoeur, "Magnetoresistive sensor in two-dimension on a 25 µm thick silicon substrate for in vivo neuronal measurements," *ACS Sensors,* 2020.
[47] T. Tapabrata, C.S. Anoop, S. Siddhartha, "linearized sigma-delta based direct digital converter for GMR sensors," *IEEE Trans. Inst. and Meas.*, vol. 70, pp. 1 – 10, 2020.
[48] E.Y. Tsymbal, D.G. Pettifor, "Perspectives of giant magnetoresistance," *Solid state physics*, vol. 56, Academic Press, pp. 113 – 237, 2001.
[49] N.J. Lewis, P.I. Anderson, Y. Gao, F. Robinson, "Development and application of measurement techniques for evaluating localized magnetic properties in electrical steel," *J. Magn. Magn. Mater.,* vol. 452, pp. 495 – 501, 2018.
[50] O. Stupakov, H. Kikuchi, T. Liu, T. Takagi, "Applicability of local magnetic measurements," *Measurements*, vol. 42, pp. 706 – 710, 2009.
[51] O. Stupakov, "Controllable magnetic hysteresis measurement of electrical steels in a single-yoke open configuration," *IEEE Trans. on Mag.,* vol. 48, n°12, pp. 4718 – 4726, 2012.
[52] IEC 60404-3, "Magnetic materials – Part 3: Methods of measurement of the magnetic properties of electrical strip and sheet by means of a single sheet tested," International Electrotechnical Commission, 2010.
[53] U. D. Annakkage, P. G. McLaren, E. Dirks, R. P. Jayasinghe and A. D. Parker, "A current transformer model based on the Jiles-Atherton theory of ferromagnetic hysteresis, " *IEEE Trans. on Pow. Deliv.*, vol. 15, no. 1, pp. 57 – 61, 2000.
[54] H. Wang and K. L. Butler, "Finite element analysis of internal winding faults in distribution transformers," *IEEE Trans. on Pow. Deliv.*, vol. 16, no. 3, pp. 422-428, 2001.
[55] J. Gyselinck, L. Vandevelde, J. Mekebeek, P. Dular, F. Henrotte, W. Legros, "Calculation of eddy currents and associated losses in electrical steel laminations," *IEEE Trans. on Mag.,* vol. 35, n°3, pp. 1191 – 1194, 1999.
[56] P. Dular, J. Gyselinck, C. Geuzaine, N. Sadowski, J.P.A. Bastos, "A 3-D magnetic vector potential formulation taking eddy currents in lamination stacks into account," *IEEE Trans. on Mag.,* vol. 39, n°3, pp. 1424 – 1427, 2008.
[57] H. Kaimori, A. Kameari, K. Fujiwara, "FEM computation of magnetic field and iron loss in laminated iron core using homogenization method," *IEEE Trans. on Mag.,* vol. 43, n°4, pp. 1405 – 1408, 2007.
[58] J.R. Brauer, Z.J. Cendes, B.C. Beihoff, K.P. Phillips, "Laminated steel eddy-current loss versus frequency computed using finite elements," *IEEE Trans. on Mag.,* vol. 36, n°4, pp. 1132 – 1137, 2000.
[59] L. Krahenbuhl, P. Dular, T. Zeidan, F. Buret, "Homogenization of lamination stacks in linear magnetodynamics," *IEEE Trans. on Mag.,* vol. 40, n°2, pp. 912 – 915, 2004.
[60] E. Lamprecht, M. Hömme, T. Albercht, "Investigations of eddy current losses in laminated cores due to the impact of various stacking processes," 2012 2nd Int. electric drives production conference (EDPC), pp. 1 – 8, 2012.
[61] J. Gyselinck, L. Vandevelde, J. Melkebeek, "Complementary two-dimensional finite element formulations with inclusion of a vectorized Jiles-Atherton model", COMPEL, 2004.
[62] A.J. Bergqvist, "A simple vector generalization of the Jiles-Atherton model of hysteresis," *IEEE Trans. on Mag.*, vol. 32, n° 5, pp. 4213 – 4215, 1996.
[63] D.C. Jiles, D.L. Atherton, "Theory of ferromagnetic hysteresis," *J. App. Phys.*, vol. 55, 6:2115, 1984.
[64] S.E. Zirka, Y.I Moroz, N. Chiesa, R.G. Harrison, and H.K. Høidalen , "Implementation of inverse hysteresis model into EMTP—Part I: Static model," *IEEE Trans. on Pow. Deliv.*, vol. 30, no. 5, pp. 2224 – 2232, 2015.
[65] S.E. Zirka, Y.I Moroz, N. Chiesa, R.G. Harrison, and H.K. Høidalen , "Implementation of inverse hysteresis model into EMTP—Part II: Dynamic model," *IEEE Trans. on Pow. Deliv.*, vol. 30, no. 5, pp. 2233 – 2241, 2015.

[66] S. Yue, P.I. Anderson, Y. Li, Q. Yang, A. Moses, “A modified inverse vector hysteresis model for nonoriented electrical steels considering anisotropy for FEA”, *IEEE Trans. on Energ. Conv.*, vol. *36, n°*4, pp.3251-3260, 2021.
[67] B. Ducharne, S. Zurek, L. Daniel, G. Sebald, “An anisotropic vector hysteresis model of ferromagnetic behavior under alternating and rotational magnetic field,” *J. Magn. Magn. Mater.,* vol. 549, 169045, 2022.